frontiers | Frontiers in Chemistry

TYPE Original Research
PUBLISHED 14 October 2024
DOI 10.3389/fchem.2024.1482168

OPEN ACCESS

EDITED BY
Yawei Yang,
Xi'an Jiaotong University, China

REVIEWED BY
Zhengqing Liu,
Northwestern Polytechnical University, China
Meidan Que,
Xi'an University of Architecture and Technology, China

*CORRESPONDENCE
Wenfei Dong,
dwf19995362248@163.com

RECEIVED 17 August 2024
ACCEPTED 20 September 2024
PUBLISHED 14 October 2024

CITATION
Dong W, Fu D, Zhang Z, Wu Z, Zhao H and Liu W (2024) Efficient electrocatalytic CO_2 reduction to ethylene using cuprous oxide derivatives. *Front. Chem.* 12:1482168.
doi: 10.3389/fchem.2024.1482168

Efficient electrocatalytic CO_2 reduction to ethylene using cuprous oxide derivatives

Wenfei Dong[1]*, Dewen Fu[1], Zhifeng Zhang[1], Zhiqiang Wu[1], Hongjian Zhao[1] and Wangsuo Liu[2]

[1]Ningxia Key Laboratory of Green Catalytic Materials and Technology, College of Chemistry and Chemical Engineering, Ningxia Normal University, Guyuan, China, [2]Department of Chemical and Environmental Engineering, Hetao College, Bayannur, Inner Mongolia, China

Copper-based materials play a vital role in the electrochemical transformation of CO_2 into C_2/C_{2+} compounds. In this study, cross-sectional octahedral Cu_2O microcrystals were prepared *in situ* on carbon paper electrodes via electrochemical deposition. The morphology and integrity of the exposed crystal surface (111) were meticulously controlled by adjusting the deposition potential, time, and temperature. These cross-sectional octahedral Cu_2O microcrystals exhibited high electrocatalytic activity for ethylene (C_2H_4) production through CO_2 reduction. In a 0.1 M $KHCO_3$ electrolyte, the Faradaic efficiency for C_2H_4 reached 42.0% at a potential of −1.376 V vs. RHE. During continuous electrolysis over 10 h, the FE (C_2H_4) remained stable around 40%. During electrolysis, the fully exposed (111) crystal faces of Cu_2O microcrystals are reduced to Cu^0, which enhances C-C coupling and could serve as the main active sites for catalyzing the conversion of CO_2 to C_2H_4.

KEYWORDS

CO_2 reduction, Cu_2O, coordination numbers, crystal surface regulation, electro-catalysis

1 Introduction

As fossil fuels continue to be exploited and used, the rising concentration of carbon dioxide has led to severe environmental issues, capturing significant public attention (Obama, 2017). Carbon capture, zero emission and reuse are considered promising strategies for processing and reducing CO_2 in the atmosphere (Lu et al., 2014). The rise of renewable energy and its important role in the field of energy has attracted people's attention. Electrocatalytic CO_2 reduction (CO_2RR) is viewed as a dependable approach to address this persistent issue. Renewable energy: Wind energy, solar energy and nuclear energy provide sustainable energy which is the continuous driving force of this strategy to realize the conversion of electrocatalytic carbon dioxide to achieve zero CO_2 emissions (Hardebeck, 2015; Liu et al., 2016).

The CO_2RR has various electrochemical products including CO, HCOOH, CH_4, C_2H_4, etc. The conversion of C_1 (CO, HCOOH) products has reached or even exceeded 90% high Faraday efficiency (Wu et al., 2020; Li et al., 2023; Li et al., 2021), while the conversion of other C_{2+} products with higher utility value does not have a high Faraday efficiency (FE) (De Luna et al., 2019). Among various electrocatalytic products, C_2H_4 has been widely used in industrial production, polymer manufacturing, and agricultural production (Loiudice et al., 2016; Ren et al., 2019), The conversion of CO_2RR to C_2H_4 is of great significance to industrial production. Currently, copper-based materials are the

sole metal substances capable of transforming carbon dioxide into ethylene and C_{2+} products using electrical energy. Despite Cu-based materials being capable of generating C_2 and C_3 products like C_2H_4, C_2H_5OH, and acetic acid, their low selectivity, high overpotential, low current density, stability, and easily affected catalytic environment prevent them from becoming highly efficient catalysts (De Luna et al., 2019; Asadi et al., 2016). This is mainly because the C_{2+} product requires the coupling of intermediates and the complex electron proton transfer process in the catalysis process, which requires a catalyst with high activity and complex morphology and structure to complete (Fan et al., 2020). The effective use of catalysts and their design play crucial roles in improving the electrocatalytic transformation of CO_2RR to ethylene. Nevertheless, the selectivity, stability, and energy efficiency of this electrocatalytic procedure require further optimization for broader industrial application.

For the design of copper-based catalysts, the current focus is mainly on heating the copper film and performing oxidation treatment, or further reduction in the process of reuse, etc. These processes are all to increase the roughness and defect degree of the copper surface (Li and Kanan, 2012; Kas et al., 2014). At the same time, in terms of improving the Cu-based catalyst, starting from the size, morphology and exposed crystal faces of the copper-based material, focus on optimizing and improving the performance of the electrocatalyst (Liu et al., 2017; Liu et al., 2022; Hori et al., 2002; Zhang et al., 2018). In the highly selective production of C_2H_4, Cu_2O NPs have better catalytic performance than metallic Cu NPs (Liu et al., 2022; Zhang et al., 2018; Ren et al., 2015; Jung et al., 2019). The recently reported Cu/Cu_2O catalyst prepared by electrodeposition has 36% FE (C_2H_4) (De Luna et al., 2018). This could be due to the fact that low-coordination Cu + ions on the surface enhance C-C coupling, which in turn supports the production of C_2H_4 (Jung et al., 2019). Recently, Kas et al. (2014) showed that Cu films derived from Cu_2O can reduce CO_2 and convert to ethylene, with FEs as high as 34–39%. The increased production of C_2H_4 on these films may be linked to the presence of the (100) Cu facet and defect sites (Kas et al., 2014; Ren et al., 2015; Hori et al., 2003). Thermal desorption studies conducted under ultra-high vacuum conditions revealed significant chemical adsorption of CO on Cu derived from Cu_2O. It is also suggested that residual CuOx species contribute to the catalytic conversion of CO_2 to C_2H_4 (Verdaguer-Casadevall et al., 2015; Kim et al., 2015). Understanding the impact of crystal faces is crucial for managing the activity and selectivity of electrocatalysts. The crystal surfaces of metallic Cu nanoparticles significantly influence the selectivity and activity in catalytic reactions. Theoretical studies indicate that an efficient catalyst should effectively facilitate the conversion of adsorbed CO protons into CHO or COH, while simultaneously displaying minimal activity for the competing hydrogen evolution reaction (Calle Vallejo and Koper, 2013). Adjusting crystal facets, particularly designing high-index crystal facets which possess numerous atomic steps, edges, and unsaturated coordination sites, offers greater potential for developing catalysts with enhanced activity and selectivity compared to merely controlling particle size (Tian et al., 2007; Zhao et al., 2018). The truncated octahedral Cu_2O nanoparticles, which include both (111) and (100) surfaces, exhibit increased selectivity towards ethylene due to a synergistic interaction among the various low-index surfaces (Gao et al., 2020). Nevertheless, there is limited research exploring the connection between the high-index surfaces of Cu-based catalysts and their CO_2RR performance (Fan et al., 2020; Gu et al., 2018). Research indicates that Cu_2O nanoparticles (NPs) with various crystal facets exhibit distinct stability and catalytic behaviors (Jiang et al., 2018; Qin et al., 2019). During the reduction phase involving Cu_2O, metallic Cu nanoparticles (NPs) develop on the Cu_2O surface. It remains uncertain if these metallic Cu NPs that form on the Cu_2O surface serve as active catalysts in the CO_2RR process (Wang et al., 2016; Lee et al., 2015). The Cu nanoparticles (NPs) derived from various types of Cu_2O NPs exhibit differences in size and aggregation, impacting the selectivity and activity involved in C_2H_4 production (Li and Kanan, 2012). These findings led us to investigate how crystal planes affect the activity of C_2H_4 formation from metallic Cu NPs derived from Cu_2O NPs, and to further examine whether the selectivity and activity of CO_2RR are influenced by Cu_2O or metallic Cu NPs.

In this work, we successfully synthesized cross-sectional octahedral Cu_2O by electrochemical deposition, and explored the potential factors of copper nanosheets derived from Cu_2O nanoparticles in electrocatalytic CO_2RR conversion to ethylene. We observed that the existence of different octahedrons on the cross-section of Cu_2O nanoparticles has a great difference in the catalytic carbon dioxide reduction of the derived copper nanosheets. Simultaneously, we examined the ethylene selectivity and activity associated with the exposed crystal surfaces. Our findings indicate that the exposure of crystal facets during the transformation of octahedral Cu_2O NPs into copper nanosheets plays a critical role in influencing the catalytic conversion of CO_2RR to ethylene. Furthermore, our studies clearly demonstrate that metallic Cu NPs, compared to Cu_2O NPs, have a greater impact on the selectivity and activity of C_2H_4. Copper nanosheets derived from Cu_2O NPs are the active species for electrocatalytic CO_2RR. For truncated octahedral Cu_2O NPs, the display of crystal planes is crucial for revealing the active material in derivatized copper nanosheets. The selectivity of CO_2 reduction, particularly towards C_2H_4, is strongly linked to the exposed crystal facets of Cu particles originating from Cu_2O.

2 Experiment

2.1 Materials and reagents

Copper nitrate ($Cu(NO_3)_2{\cdot}3H_2O$, ≥99.5% pure) was sourced from Beijing Chemical Plant of China Reagent, while sodium acetate ($C_2H_3NaO_2$, ≥99.0% pure) and sodium hydroxide (NaOH, 99%) were obtained from Macklin Reagent Network. Acetic acid (CH_3COOH, ≥99.5% pure) and potassium bicarbonate ($KHCO_3$, ≥99.5% pure) were procured from Sinopharm Chemical Reagent Co., Ltd. No additional

purification of these chemicals is required. The deionized water used (18.24 MΩ cm) was produced by our laboratory's ultra-pure water system.

2.2 Synthesis of catalyst

The electrolytic cell and electrodes used are as follows: a standard three-electrode device, the constant potential method is used for electrodeposition on the workstation of the electrochemical system (CH 760E, CH Instruments, China). The working electrode is carbon paper (0.5 cm^2, Toray TGP-H-060), using AgCl or Ag/Ag^+ electrode and platinum sheet as reference electrode and counter electrode.

The electroplating solution is an aqueous solution composed of 0.02 M (Cu $(NO_3)_2{\cdot}3H_2O$ and 0.12 M acetic acid buffer solution, and the pH is adjusted to about 5.0 with sodium hydroxide. Electrodeposition is electrolysis in an H-type double-layer constant temperature water bath The Cu_2O electrocatalyst was synthesized by constant potential method under 70°C water circulation and recorded as 0.02–1,500 (0.02-represents the potential. 1,500 represents the settling time). Each time the deposited Cu_2O carbon paper sheet, use deionized water thoroughly Clean and blow dry with nitrogen.

2.3 Equipment

The sample's crystal structure was analyzed using an X-ray diffractometer (Smart Lab, Japan) with intelligent target rotation capability. Surface morphology of each electrocatalyst was examined using a cold field emission scanning electron microscope (F-SEM, Regulus 8100, Japan) and high-resolution transmission electron microscopy (HRTEM, JEM-2100uHR, Japan). Elemental analysis was performed with X-ray photoelectron spectroscopy (XPS, Thermo Scientific K-Alpha, US), employing a monochromatic AlKa radiation source at 1,486.6 eV. All the spectral data were acquired in standard environmental conditions.

2.4 Electrochemical test

Electrocatalysis is conducted using a standard H-type electrolysis cell that has three electrodes linked to an electrochemical workstation (CH 760E, CH Instrument, China). The device features a cathode and an anode compartment divided by a proton exchange membrane (Nafion 130). Each section holds 30 mL of 0.1 M $KHCO_3$ as the electrolyte solution. Reference electrodes and counter electrodes were comprised of AgCl or Ag/Ag^+ electrodes and platinum sheets, respectively. A self-fabricated electrode was employed as the working electrode. Following this, the products of the electrocatalytic reduction process were analyzed over 30 min via a chronocurrent technique. All electrical potentials noted in this experiment are calibrated against the Ag/AgCl reference electrode as E (VS RHE) = E (VS Ag/AgCl) + 0.222 V + 0.0591 × pH.

2.5 Product detection

Prior to conducting the experiment, the cathode chamber was set up with an online trace gas detection system for CO_2 reduction using gas chromatography (GC) (GC7900, Tianmei, China). This system includes a thermal conductivity detector (TCD) and a flame ionization detector (FID), with nitrogen serving as the carrier gas to analyze and quantify the resultant products. The electrolyte within the cathode chamber was saturated with N_2 or CO_2 at a flow rate of 30 mL min^{-1} for no less than 30 min. Concurrent magnetic stirring at 600 rpm during the process ensured thorough mixing of the electrolyte. Linear sweep voltammetry (LSV) recordings were taken at a scan rate of 10 mV s^{-1}. Electrochemical surface area (ECSA) was derived from cyclic voltammograms at varying scan rates (5, 10, 20, 40, 60, 80, 100, and 120 mV s^{-1}), within potential window from −0.116 to −0.216 vs. RHE. Electrochemical impedance spectroscopy was conducted in a frequency range of 1 MHz to 10^{-2} Hz under open circuit potential.

Then the quantitative gas products were analyzed for at least 30 min at each potential during the CO_2 electroreduction process. Based on the GC analysis, the current density and FE of the product were determined. The liquid product underwent further analysis. The FE for CO is calculated using the formula below:

$$FE = \frac{NnF}{Q} \times 100\%$$

Here, (N) represents the number of electrons needed to synthesize the product, which equals 2 for C_2H_4. The variable (n) stands for the total moles of C_2H_4 as measured by GC, (F) is the Faraday constant (96,485°C mol^{-1}), and (Q) denotes the total accumulated electric charge. These details are recorded using ChemStation.

3 Results and discussion

3.1 Physical characteristics of nanomicrocrystals

A straightforward constant potential electrochemical deposition technique was utilized to effectively cultivate Cu_2O particles directly on carbon paper (CP), serving as electrodes with a carbon base. A self-supported electrode like Cu_2O/CP was prepared. The electrodeposition was carried out in an H-type double-layer constant-temperature water-bath electrolyzer, and the Cu_2O electrocatalyst was synthesized using the constant-potential method under water circulation at 70°C notated as Cu_2O 0.02–1,500 (70°C) (0.02- represents the electrodeposition potential, 1,500 represents the deposition time, and 70°C represents the electrodeposition temperature) as shown in Figure 1A. The Cu_2O microcrystals on the carbon paper (CP) surface were uniformly distributed and have a polycrystalline octahedral morphology (shown in the inset of Figure 1A) with typical (111) and (100) crystal faces. Electrodeposition was performed at temperatures of 60°C and 80°C to establish comparative conditions, with SEM images of the resulting materials presented in Figures 1B, C. The materials

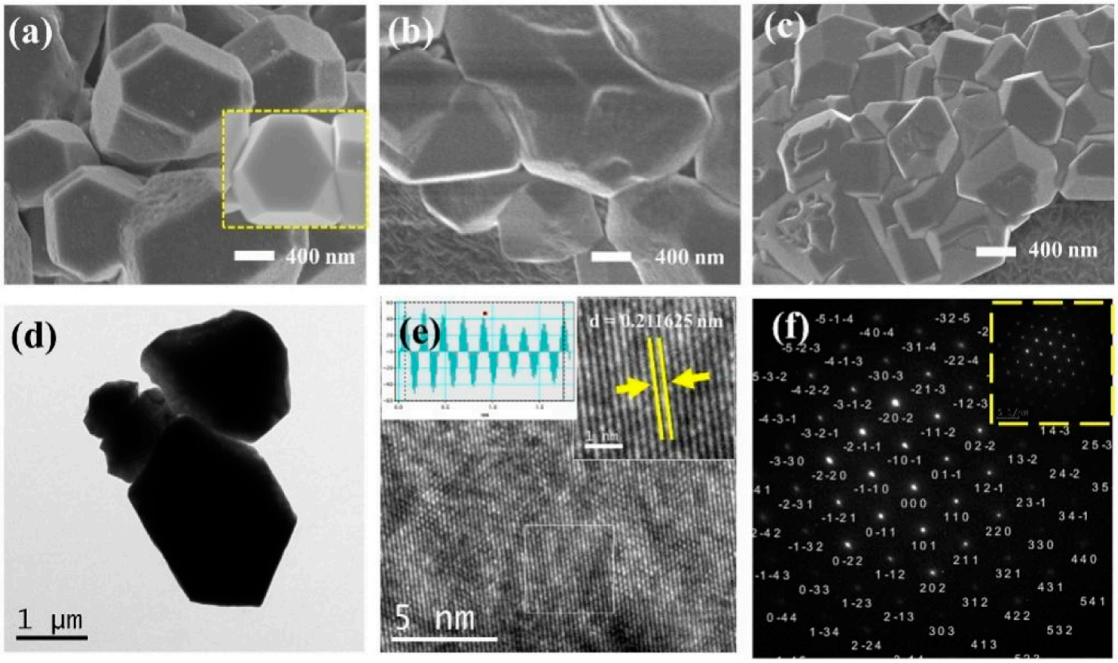

FIGURE 1
SEM images of Cu_2O (0.02–1,500) at different electrodeposition temperatures **(A)** 70°C, **(B)** 60°C and **(C)** 80°C; Cu_2O (0.02–1,500) (70°C) **(D)** TEM images, **(E)** HRTEM images, **(F)** SAED images.

electrodeposited at 60°C are specifically depicted in Figures 1B, C. The Cu_2O microcrystalline particles deposited at 60°C are uniformly distributed, but do not have a complete octahedral morphology, and the Cu_2O microcrystalline particles obtained by deposition at 80°C are piled up together, and the crystalline faces of the cross-sectional octahedra are incompletely exposed, with only some of the crystalline faces being exposed and the other crystalline faces interspersed with each other to hide them. Comparison of the electrodeposition temperatures reveals that the Cu_2O microcrystals are uniformly distributed and the crystal faces are well exposed at 70°C. To further explore the microstructural characteristics, TEM images of the Cu_2O catalyst are displayed in Figure 1D, while the HRTEM and SAED (selected area electron diffraction) images are illustrated in Figures 1E, F. The TEM images illustrate clearly defined crystal faces of Cu_2O particles. The marked lattice stripe distance d of 0.212 nm aligns with the crystal face spacing of Cu_2O, and the SAED patterns observed highlight the (111) and (100) crystal planes of the octahedral cross-section of Cu_2O. Figure 2 shows the SEM images of Cu_2O (0.02–70) at different electrodeposition times, demonstrating the effect of electrodeposition time on the morphology, and determining that 1,500 scan electrodeposit Cu_2O with a more complete crystal surface.

Figure 3A presents the X-ray diffraction (XRD) pattern. The figure indicates that the Cu_2O microcrystals, electrodeposited directly onto the CP substrate, did not fully coat the surface of the carbon paper, and the XRD signal peaks of the carbon paper were observable in the XRD spectrum (▲: denotes the CP diffraction peaks). The main signal peaks of the Cu_2O crystal structure (◎: denotes the Cu_2O signal peaks) were in agreement with the standard spectrum (Cu_2O: JCPDS #05-0667) against (Liu et al., 2021). The diffraction peaks of Cu_2O microcrystals at 29.554 eV, 36.418 eV, 42.297 eV, 61.344 eV, 73.526 eV, and 77.323 eV were attributed to the (110), (111), (200), (220), (311), and (222) crystallographic facets of Cu_2O, respectively. It indicates that the Cu_2O catalyst has good crystallinity and structural characteristics of polycrystalline facets.

The surface valence states of the catalyst were examined using X-ray photoelectron spectroscopy (XPS). As depicted in Figures 3B, 4A, the Cu_2O microcrystals electrodeposited *in situ* with CP as the substrate contain characteristic peaks of Cu 2p and O 1s, as well as information on the elements contained in the substrate carbon paper. The characteristic peaks with binding energies of 931.88 eV and 951.78 eV are attributed to Cu^+ $2p^{3/2}$ and Cu^+ $2p^{1/2}$, which can be categorized as (Cu^+) of Cu_2O. The predominant Cu^{2+} $2p^{3/2}$ and Cu^{2+} $2p^{1/2}$ features at 934.28 eV and 954.08 eV can be attributed to the presence of (Cu^{2+}) or a small amount of CuO in Cu_2O. Satellite peaks appear in the binding energy range of 945 eV–940 eV, indicating that Cu(I) is the primary valence state of the copper species. The presence of Cu (II) results from the oxidation of Cu(I), as Cu_2O is thermodynamically unstable under typical conditions. Figures 4C, D It can be determined that Cu_2O obtained at different deposition temperatures: 0.02–1,500 (60°C), 0.02–1,500 (70°C), 0.02–1,500 (80°C) are homogeneous compounds, and by comparing the SEM as in Figures 1–5 a great difference in morphology is found.

3.2 Electrochemical CO_2 reduction properties of Cu_2O microcrystals

The electrocatalytic CO_2 reduction performance of Cu_2O 0.02–1,500 (70°C) was evaluated as illustrated in Figure 5A. This

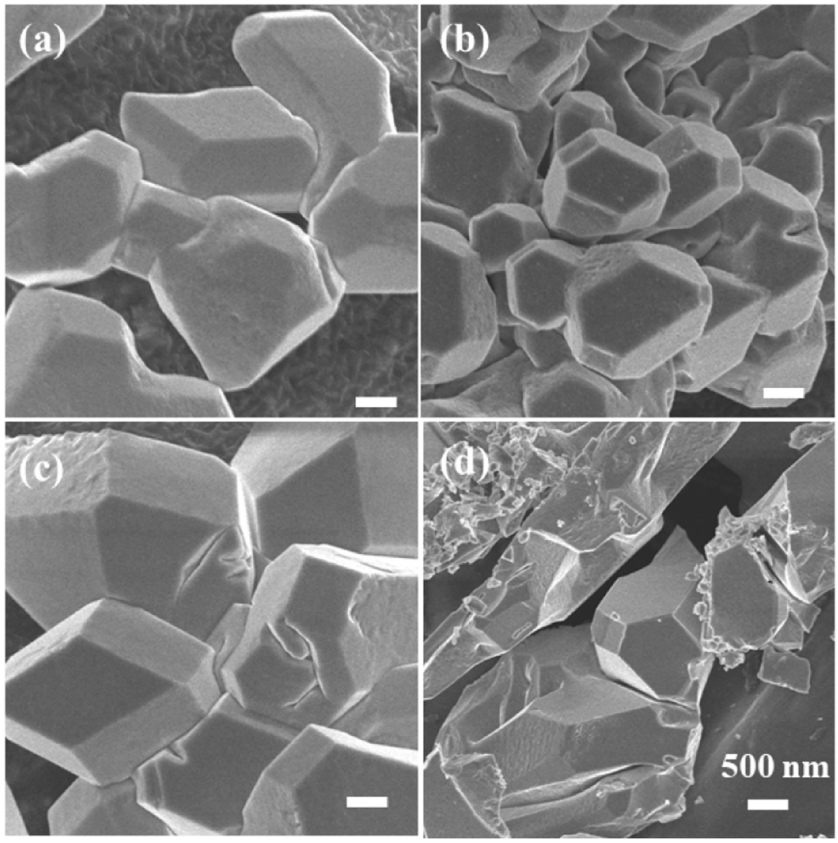

FIGURE 2
SEM images of Cu_2O (0.02–70) at different electrodeposition times, **(A)** 1,300 s, **(B)** 1,500 s, **(C)** 1,800 s and **(D)** 3,600 s.

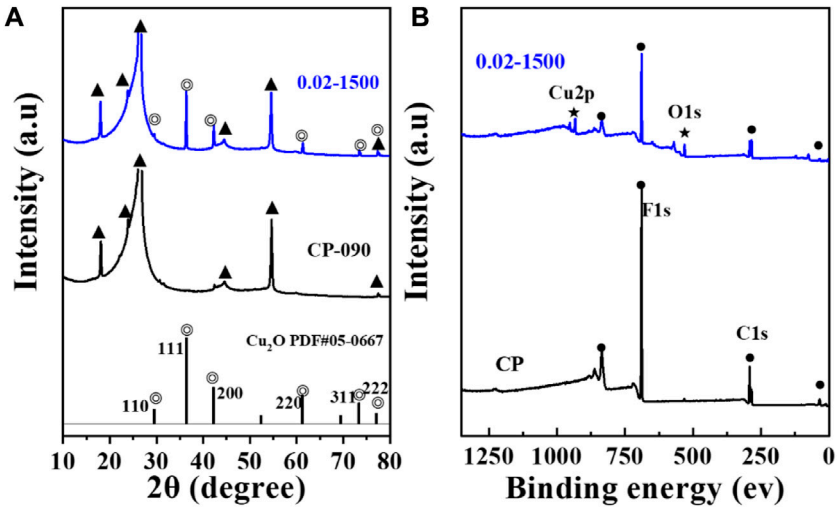

FIGURE 3
(A) XRD pattern of Cu_2O (0.02–1,500) and CP, **(B)** XPS spectra of Cu_2O (0.02–1,500) and CP.

catalyst was tested in a 0.1 M $KHCO_3$ solution saturated with both CO_2 and Ar, where it exhibited a significant reduction peak from −0.25 V to −0.5 V (vs. RHE), likely due to the inherent electrochemical reduction properties of Cu_2O. Additionally, the intensity of these reduction peaks was higher in the CO_2-saturated environment compared to the Ar-saturated one, indicating more pronounced reduction activities in the presence of CO_2. This enhanced peak is believed to result from the elevated

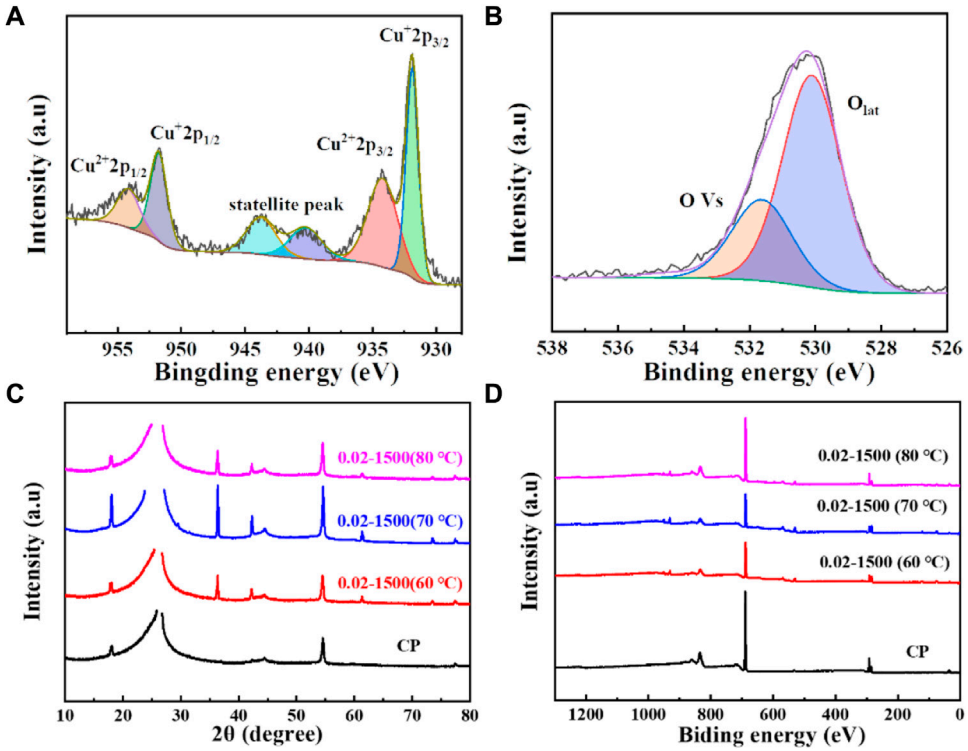

FIGURE 4
(A) Cu 2p spectrum of Cu_2O (0.02–1,500) (70°C); **(B)** O1 s spectrum of Cu_2O (0.02–1,500) (70°C); **(C)** XRD pattern of Cu_2O; **(D)** XPS spectra of Cu_2O.

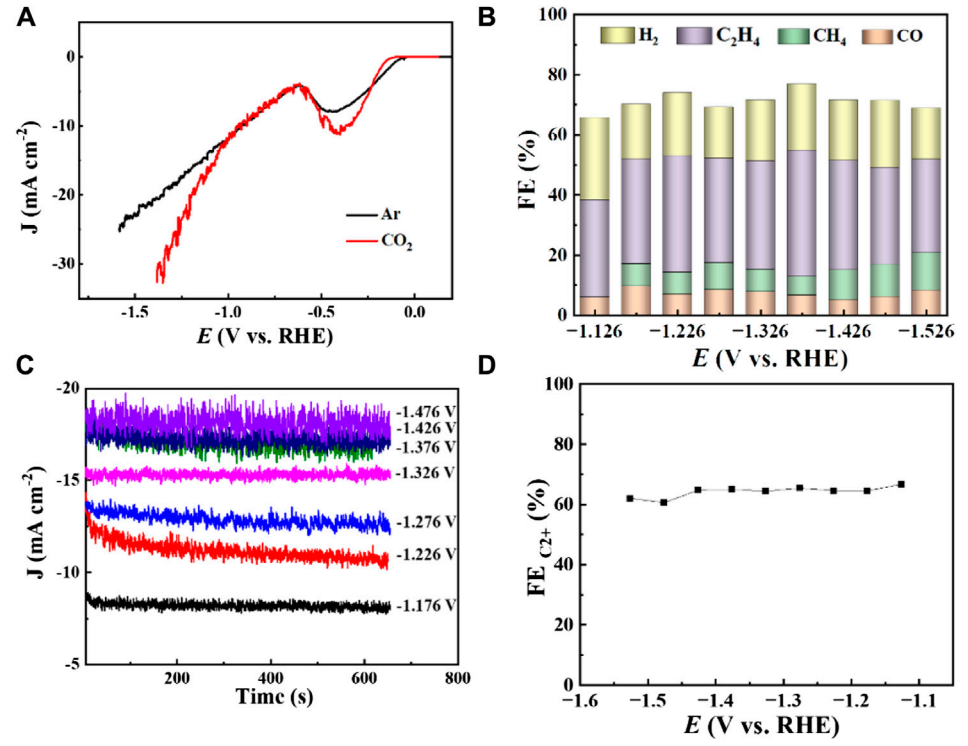

FIGURE 5
Cu_2O 0.02–1,500 (70°C) **(A)** LSV curves at CO_2 and Ar saturated 0.1 M $KHCO_3$ with a scan rate of 10 mV s^{-1}, **(B)** FE of CO_2 reduction of different products at different potentials, **(C)** Total current density at different reduction potentials, **(D)** FE of CO_2 reduction products C_{2+} at different potentials.

TABLE 1 Performance of different copper-based catalysts for C_2H_4 formation via electrochemical CO_2 reduction.

Catalyst	Electrolyte	Potential	Product	FE (%)	References
Cu_2O nanocubes	0.1 M $KHCO_3$	−1.15 V vs. RHE	C_2H_4	31.1	Wang et al. (2019)
Graphene/ZnO/Cu_2O	0.5 M $NaHCO_3$	−0.9 V vs. Ag/AgCl	n-propanol	30	Geioushy et al. (2017a)
Cu_2O/Cu@NC	0.1 M $KHCO_3$	−0.68 V vs. RHE	HCOOH	70.5	Li et al. (2020)
Cu@Cu_2O	0.1 M $KHCO_3$	−1.0 V vs. RHE	C2 = C2 (ethylene and ethanol)	50	Shang et al. (2019)
Cu GNC-VL	0.5 M $KHCO_3$	−0.87 V vs. RHE	Ethanol	70.52	Zhang et al. (2019)
In-doped Cu@Cu_2O	0.1 M $KHCO_3$	−0.8 V vs. RHE	CO	87.6 ± 2.2	Wang et al. (2020)
cubic Cu_2O (c-Cu_2O) NPs with facets	0.5 M $KHCO_3$	−1.2 V vs. RHE	C_2H_4	38	Gao et al. (2020)
octahedral Cu_2O (o-Cu_2O) NPs	0.5 M $KHCO_3$	−1.1 V vs. RHE	C_2H_4	45	Robb (2021)
truncated-octahedral Cu_2O (t-Cu_2O) NPs with both and (100) facets	0.5 M $KHCO_3$	−1.1 V vs. RHE	C_2H_4	59	Robb (2021)
Cu_2O-BDD	0.1 M NaCl	−1.5 V vs. RHE	C_2H_4	68.2	Denala et al. (2019)
Cuv-Cu_2O catalyst	0.1 M $KHCO_3$	−0.76 V vs. RHE	C_2H_4	51.0	Ren et al. (2020)
Cu_2O (o-Cu_2O) NCs	1.0 M KCl	−1.1 V vs. RHE	C_{2+}	48.3	Fu et al. (2020)
Hollow Cubic Cu_2O@Au	0.1 M $KHCO_3$	−1.0 V vs. RHE	CO	30.1	Tan et al. (2019)
Cu_2O-derived Cu catalysts	0.1 M $KHCO_3$	−0.98 V vs. RHE	C_2H_4	42.6	Handoko et al. (2016)
Cu_2O/CuO	0.5 M $KHCO_3$, 10 mM pyridine and HCl (pH = 5)	−1.3 V vs. RHE	CH_3OH	6.46	Roy et al. (2020)
GN/Cu_2O	0.5 M $NaHCO_3$	−0.9 V vs. Ag/AgCl	C_2H_5OH	9.93	Geioushy et al. (2017b)
ZnO@4Cu_2O	1 M KOH	−1.0 V vs. RHE	C_2H_4	35.5	Zhu et al. (2021)
Cu/Cu_2O-Ag-x)	1 M KOH	200 mA cm^{-2}	C_{2+}	60.9	Su et al. (2021)
Cu/Cu_2O@NG	0.2 M KI	−1.9 V vs. RHE	C_2-C_3	56	Zhi et al. (2021)
AuxCu_2O	0.1 M $KHCO_3$	−1.3 V vs. RHE	C_2H_4	24.4	Cao et al. (2021)

CO_2 concentration within the CO_2-saturated medium versus the Ar-saturated solution. Across a broad potential range, the current density of the catalyst Cu_2O 0.02–1,500 (70°C) in the CO_2-enriched 0.1 M $KHCO_3$ solution surpassed that in its Ar-saturated counterpart, demonstrating the robust catalytic reduction capabilities of Cu_2O microcrystals in CO_2-rich environments.

The FE of various gaseous products (H_2, CO, CH_4, C_2H_4) produced by CO_2 reduction using Cu_2O 0.02–1,500 (70°C) were evaluated at different potentials in a 0.1 M $KHCO_3$ electrolyte, as shown in Figure 5B. The highest FE, reaching 42%, was observed for C_2H_4 at a potential of −1.376 V (vs. RHE) with a total current density of 17 mA cm^{-2}, which suggests strong selectivity of the catalyst towards C_2H_4 production. Figure 5C illustrates the distribution of total current density across various potentials, indicating an increase in total current density with higher reduction potentials. Figure 5D presents the overall FE of the CO_2 reduction product C_{2+} at various potentials for the 0.02–1,500 (70°C) catalysts under a 0.1 M $KHCO_3$ electrolyte setting, where the FE for C_{2+} products was approximately 60% across all tested potentials. In conclusion, C_2H_4 is identified as the primary product of CO_2 electroreduction, indicating that the Cu_2O microcrystalline particles have good active sites for the generation of C_{2+} during the CO_2 electroreduction process. The Cu_2O 0.02–1,500 (70°C) catalysts achieved 42.0% FE (C_2H_4) and more than 60% FE (C_{2+}). Table 1 summarizes the FE of copper-based catalysts for C_2H_4 production. The comparison reveals that Cu_2O microcrystalline particles prepared *in situ* by electrodeposition are one of the more desirable catalysts for ethylene production by electrocatalytic reduction of CO_2.

Increased current density in a CO_2-saturated electrolyte suggested an electrochemical CO_2 reduction reaction (CO_2RR). Analysis using gas chromatography (GC) revealed the production of C_2H_4, CH_4, CO, and H_2. The catalyst 0.02–1,500 (70°C) demonstrated significant selectivity towards C_2H_4, achieving a faradaic efficiency (FE) of 42.0% at a current density of 7.3 mA cm^{-2} and a potential of −1.376 V (vs. RHE), as shown in

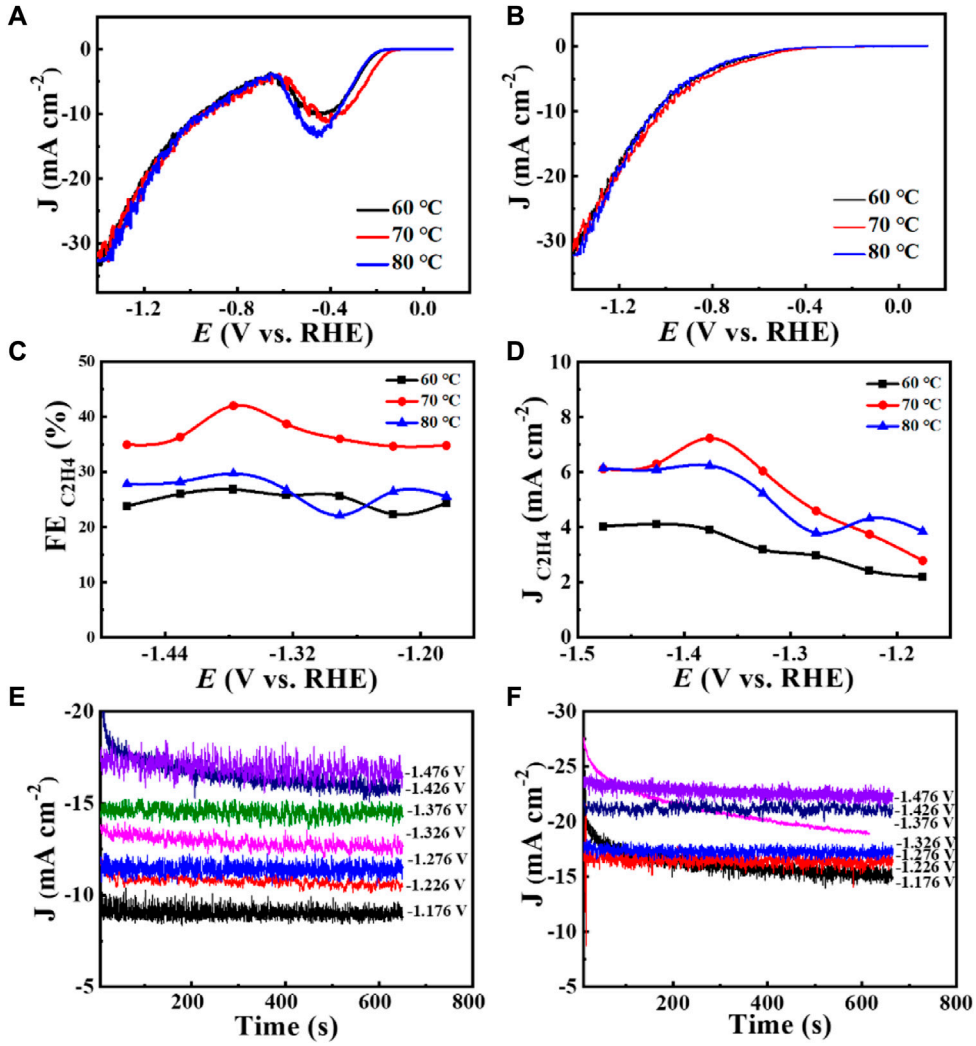

FIGURE 6
Catalyst Cu_2O 0.02–1,500 (60°C, 70°C, 80°C): **(A)** 1st LSV curve at CO_2 and Ar saturated 0.1 M $KHCO_3$ with a scan rate of 10 mV s^{-1}, **(B)** 2nd LSV curve at CO_2 and Ar saturated 0.1 M $KHCO_3$ with a scan rate of 10 mV s^{-1}, **(C)** FE (C_2H_4) values as a function of potential, **(D)** J (C_2H_4) values as a function of potential, **(E)** Total current density at different reduction potentials from 0.02 to 1,500 (60°C), **(F)** Total current density at different reduction potentials for Cu_2O 0.02–1,500 (80°C).

Figure 6. The measurement of FE (C_2H_4) was repeated three times to obtain a FE (C_2H_4) of 42% with good reproducibility. Figure 7 demonstrates that the catalyst Cu_2O 0.02–1,500 (70°C) has the optimal theoretical electroactive area, and Figure 8 shows the optimal electron transfer rate for the catalyst Cu_2O 0.02–1,500 (70°C), which are based on the comparison of synthesized catalysts at other temperatures. During 10 h of continuous catalytic use the FE remained essentially undecayed at about 40% as shown in Figure 9.

3.3 Catalytic mechanism study

We tested the morphology of Cu_2O catalysts after electrochemical CO_2 reduction reaction, as shown in Figure 10. The Cu_2O catalysts after electrolysis failed to maintain the original cross-sectional octahedral morphology. The Cu_2O catalysts formed nanosheet morphology during the electrolysis process, which may be due to the reduction of Cu_2O at a more negative potential. Figures 11A, 12C show that many of the original crystalline surfaces of the Cu_2O microcrystals obviously disappeared after electrochemical CO_2 reduction, which further proved that Cu_2O was reduced during the electrochemical reaction. From the XPS spectra in Figures 11B, 12A, it can be seen that the characteristic peak areas of Cu^+ and Cu^{2+} of the Cu catalyst obtained after being reduced compared with the characteristic peaks of Cu^+ and Cu^{2+} in the Cu_2O catalyst (Figure 4A), and the proportion of the peak areas of Cu^+ $2p^{3/2}$ and Cu^+ $2p^{1/2}$ of the Cu catalyst obtained from the reduced Cu_2O was reduced, proving that Cu+ and Cu^{2+} in the catalyst were reduced to Cu0 and Cu+. Figure12B depicts the high-resolution O1s spectra of the prepared Cu_2O:0.02–1,500

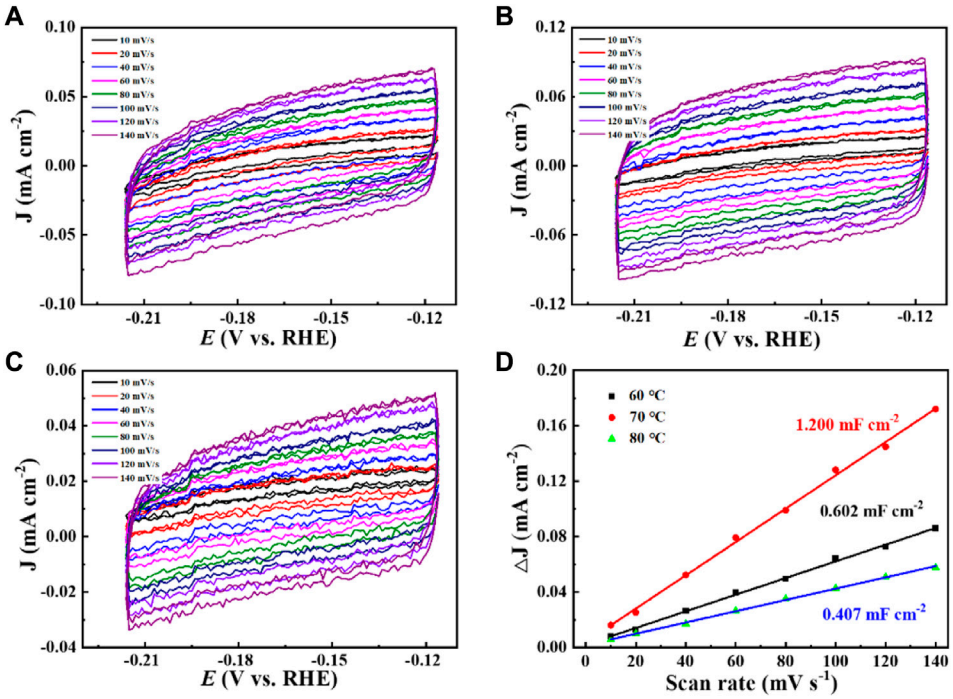

FIGURE 7
The CVs of **(A)** Cu_2O 0.02–1,500 (60°C), **(B)** Cu_2O 0.02–1,500 (70°C), and **(C)** Cu_2O 0.02–1,500 (80°C), **(D)** Bilayer charge current densities of Cu_2O 0.02–1,500 (60°C), Cu_2O 0.02–1,500 (70°C), and Cu_2O 0.02–1,500 (80°C) versus scan rate.

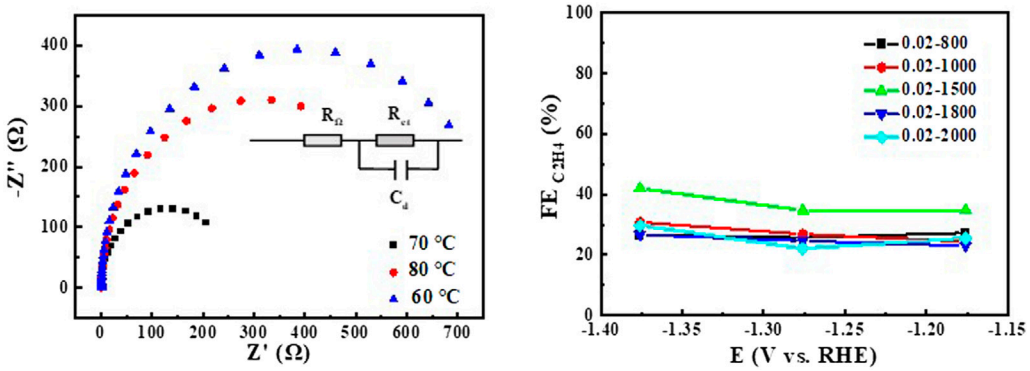

FIGURE 8
EIS of Cu_2O 0.02–1500 (60°C, 70°C 0, 80°C) at open circuit voltage for CO_2 saturated 0.1 M $KHCO_3$, relationship between FE of the product ethylene and the potential of CO_2 reduction for Cu_2O.

(70°C) catalysts after the electrochemical CO_2 reduction reaction. As shown in Figure 4B, the two characteristic peaks resolved at 529.95 eV and 531.33 eV binding energies are Cu_2O lattice oxygen (Olat) and oxygen vacancies (OVs), respectively. After the electrochemical CO_2 reduction reaction, there are oxygen vacancies (OVs) at the binding energy of 531.33 eV, while the Cu_2O lattice oxygen (O lat) basically disappears, as shown in Figure 12B. The Auger electron spectroscopy (AES) Cu LMM signals of Cu_2O 0.02–1,500 (70°C) (Figure 12D), at the binding energy of 570.8 eV, show a characteristic peak, which confirms that Cu(I) is the major chemical valence of Cu species. After the electrochemical CO_2 reduction reaction, a characteristic peak at the binding energy of 570.8 eV is shown, which confirms that Cu (0) is the main chemical valence of the Cu species after derivatization. This proves that the catalyst Cu_2O is derivatized to Cu^0 species after electrochemical CO_2 reduction reaction.

By comparing the CO_2 reduction performance of Cu_2O catalysts under different preparation conditions, Cu_2O 0.02–1,500 (70°C) with regular morphology and the most intact cross-sectional octahedra with exposed crystal faces (111) has a higher selectivity for the conversion of CO_2 to

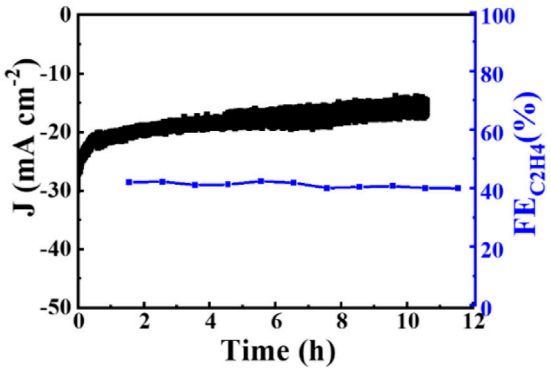

FIGURE 9
The stability of Cu_2O 0.02–1,500 (70°C) Cu_2O in 0.1 M $KHCO_3$ electrolyte at −1.376 V (vs. RHE).

During the CO_2 electroreduction process, *CO is considered to an important intermediate which is further reduced to C_2H_4 over Cu_2O-based catalysts. For C_2/C_{2+} products, this phenomenon may be attributed to the severe aggregation of *CO on the surface of the catalysts' Cu_2O-reduced derivatives promoting further C-C coupling. Cu(I) can be reduced to Cu (0) during the catalytic process, so the center of catalytic activity is viewed as a derivative catalyst with Cu (0). In summary, the active substance in the reduced electrocatalytic conversion of CO_2 by Cu_2O is the reduced derived Cu (0).

3.4 Conclusion

Cross-sectioned octahedral Cu_2O microcrystals were prepared *in situ* on carbon paper electrodes by electrochemical deposition. The morphology and integrity of the exposed crystal surface (111) were successfully regulated by controlling the deposition potential, deposition time and deposition temperature. The cross-sectional octahedral Cu_2O microcrystals have high activity and selectivity for the preparation of C_2H_4 by electrocatalytic CO_2 reduction. The FE (C_2H_4) was stabilized at about 40% during 10 h of continuous electrolysis. The cross-sectioned octahedral Cu_2O microcrystals with intact exposed crystal faces (111) are reduced derived Cu0 during electrolysis, which can effectively promote C-C coupling and may be the main active site for catalyzing the conversion of CO_2 to C_2H_4.

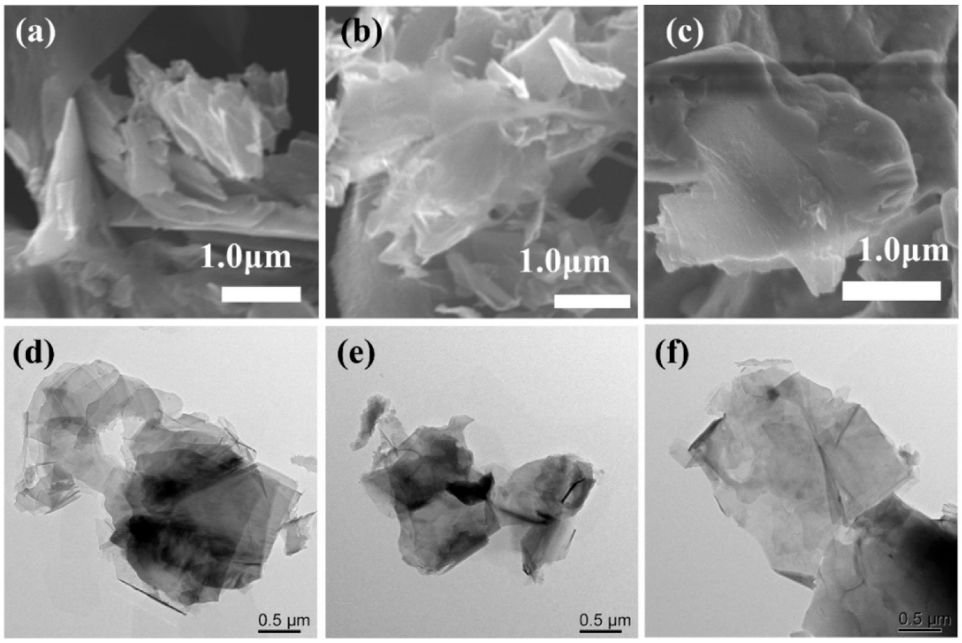

FIGURE 10
SEM images of **(A)** 0.02–1,500 (60°C), **(B)** Cu_2O 0.02–1,500 (70°C) and **(C)** Cu_2O 0.02–1,500 (80°C) catalysts after use. TEM images of **(D)** Cu_2O 0.02–1,500 (60°C), **(E)** Cu_2O 0.02–1,500 (70°C) and **(F)** Cu_2O 0.02–1,500 (80°C) catalysts after use.

C_2H_4. The complete exposure of crystal faces is particularly important for electrocatalytic conversion of CO_2 to C_2H_4 and is an important factor affecting the increase of FE (C_2H_4).C-C coupling is a crucial step in electrocatalytic conversion of CO_2 to C_2H_4, and intermediate adsorption completes the coupling of C-C to C_2/C_{2+} products. The Cu_2O 0.02–1,500 (70°C) catalysts with a Cu_2O 0.02–1,500 (70°C) catalysts with complete morphology and exposed (111) crystal surface are the key active sites for C-C coupling in the catalytic process. The derivatives obtained by a reduction of the catalyst with well exposed crystalline surfaces are the key active sites for the catalytic conversion of CO_2 into C_2H_4 (Gao et al., 2020).

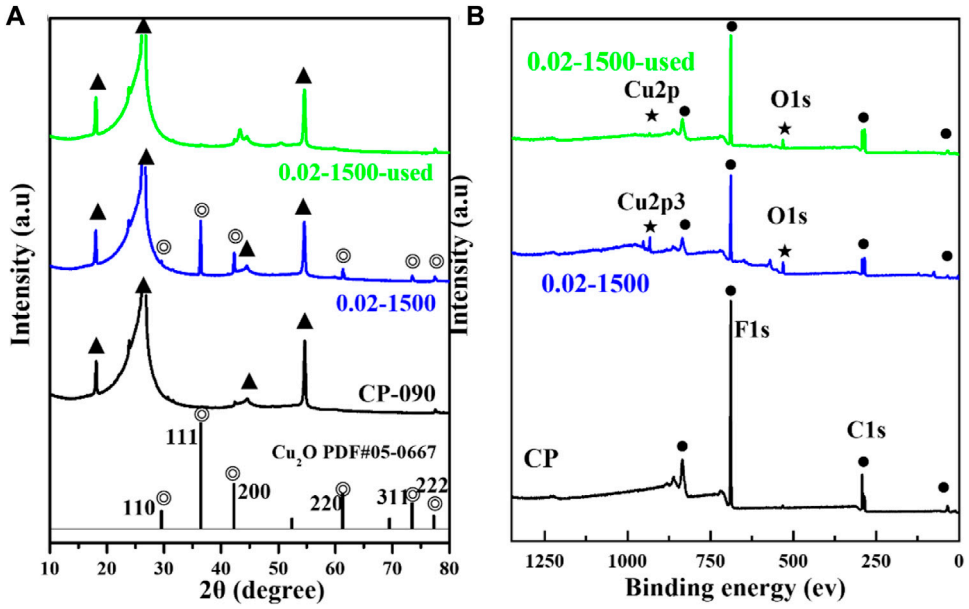

FIGURE 11
(A) Cu_2O (0.02–1,500), Cu_2O (0.02–1,500) after being used, and XRD spectra of CP, **(B)** Cu_2O (0.02–1,500), Cu_2O (0.02–1,500) after being used, and XPS spectra of CP.

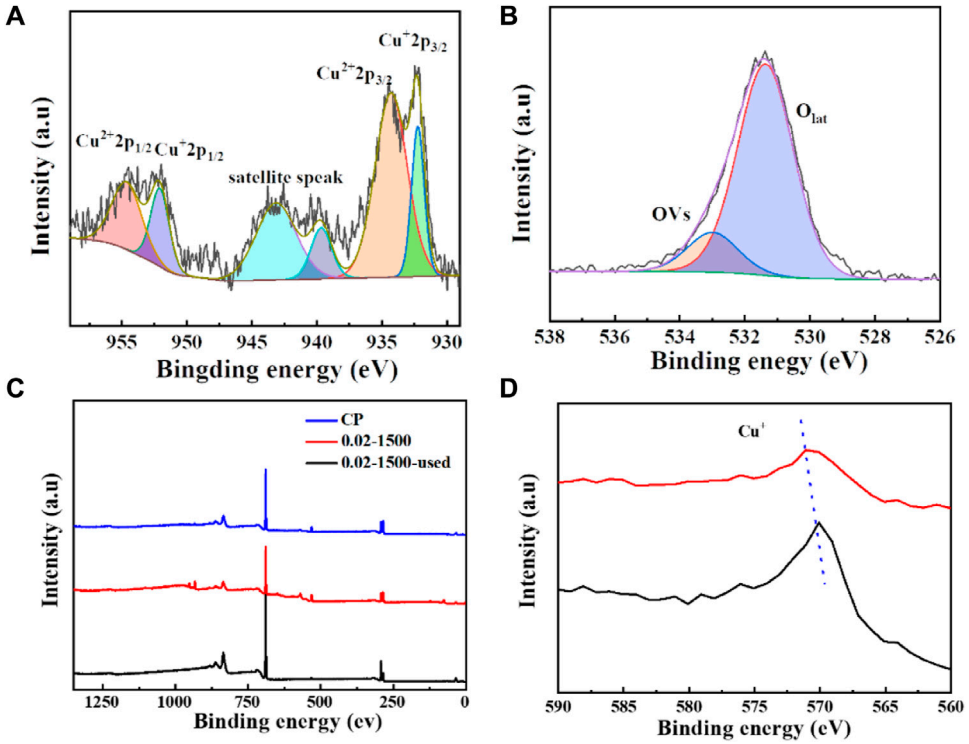

FIGURE 12
(A) 0.02–1,500 (70°C) Cu 2p spectra, **(B)** 0.02–1,500 (70°C) O 1 s spectra, **(C)** CP, 0.02–1,500 (70°C), and 0.02–1,500 (70°C) were used after the spectra XPS spectra **(D)** 0.02–1,500 (70°C) and 0.02–1,500 (70°C) were used Cu LM2 spectra after being used.

Data availability statement

The original contributions presented in the study are included in the article/supplementary material, further inquiries can be directed to the corresponding author.

Author contributions

WD: Conceptualization, Data curation, Formal Analysis, Funding acquisition, Investigation, Methodology, Project administration, Resources, Software, Supervision, Validation, Visualization, Writing–original draft, Writing–review and editing. DF: Writing–original draft, Writing–review and editing. ZZ: Conceptualization, Data curation, Formal Analysis, Funding acquisition, Investigation, Methodology, Project administration, Resources, Software, Supervision, Validation, Visualization, Writing–original draft, Writing–review and editing. ZW: Conceptualization, Data curation, Formal Analysis, Funding acquisition, Investigation, Methodology, Project administration, Resources, Software, Supervision, Validation, Visualization, Writing–original draft, Writing–review and editing. HZ: Conceptualization, Data curation, Formal Analysis, Funding acquisition, Investigation, Methodology, Project administration, Resources, Software, Supervision, Validation, Visualization, Writing–original draft, Writing–review and editing. WL: Writing–original draft, Writing–review and editing.

Funding

The author(s) declare financial support was received for the research, authorship, and/or publication of this article. This work was financially supported by the National Natural Science Foundation of China Grant Nos 22262027 and 22132003), the Scientific Research Project of Higher Education Institutions of Ningxia Autonomous Region, NYG2024203, 2023 University level Research Project of Ningxia Normal University (XJZDD2324) and Research Project of School of Chemistry and Chemical Engineering, Ningxia Normal University (HGZD23-04).

Conflict of interest

The authors declare that the research was conducted in the absence of any commercial or financial relationships that could be construed as a potential conflict of interest.

Publisher's note

References

Asadi, M., Kim, K., Liu, C., Addepalli, A. V., Abbasi, P., Yasaei, P., et al. (2016). Nanostructured transition metal dichalcogenide electrocatalysts for CO_2 reduction in ionic liquid. *Science* 353 (6298), 467–470. doi:10.1126/science.aaf4767

Calle Vallejo, F., and Koper, M. T. (2013). Theoretical considerations on the electroreduction of CO to C_2 species on Cu (100) electrodes. *Angew. Chem.* 125 (28), 7423–7426. doi:10.1002/ange.201301470

Cao, X., Cao, G., Li, M., Zhu, X., Han, J., Ge, Q., et al. (2021). Enhanced ethylene formation from carbon dioxide reduction through sequential catalysis on Au decorated cubic Cu_2O electrocatalyst. *Eur. J. Inorg. Chem.* 2021 (24), 2353–2364. doi:10.1002/ejic.202100229

De Luna, P., Hahn, C., Higgins, D., Jaffer, S. A., Jaramillo, T. F., and Sargent, E. H. (2019). What would it take for renewably powered electrosynthesis to displace petrochemical processes? *Science* 364 (6438), eaav3506. doi:10.1126/science.aav3506

De Luna, P., Quintero-Bermudez, R., Dinh, C.-T., Ross, M. B., Bushuyev, O. S., Todorović, P., et al. (2018). Catalyst electro-redeposition controls morphology and oxidation state for selective carbon dioxide reduction. *Nat. Catal.* 1 (2), 103–110. doi:10.1038/s41929-017-0018-9

Denala, D., Khalil, M., and Ivandini, T. A. (2019). "Preparation of boron doped diamond modified with cuprous oxide as working electrode for electroreduction of CO_2," in Proceedings of the 4th international symposium on current progress in mathematics and sciences (Iscpms2018), Depok, Indonesia.

Fan, L., Xia, C., Yang, F., Wang, J., Wang, H., and Lu, Y. (2020). Strategies in catalysts and electrolyzer design for electrochemical CO_2 reduction toward C_{2+} products. *Sci. Adv.* 6 (8), eaay3111. doi:10.1126/sciadv.aay3111

Fu, W., Liu, Z., Wang, T., Liang, J., Duan, S., Xie, L., et al. (2020). Promoting C_{2+} production from electrochemical CO_2 reduction on shape-controlled cuprous oxide nanocrystals with high-index facets. *ACS Sustain. Chem. and Eng.* 8 (40), 15223–15229. doi:10.1021/acssuschemeng.0c04873

Gao, Y., Wu, Q., Liang, X., Wang, Z., Zheng, Z., Wang, P., et al. (2020). Cu_2O nanoparticles with both {100} and {111} facets for enhancing the selectivity and activity of CO_2 electroreduction to ethylene. *Adv. Sci. (Weinh)* 7 (6), 1902820. doi:10.1002/advs.201902820

Geioushy, R. A., Khaled, M. M., Alhooshani, K., Hakeem, A. S., and Rinaldi, A. (2017a). Graphene/ZnO/Cu_2O electrocatalyst for selective conversion of CO_2 into n-propanol. *Electrochimica Acta* 245, 456–462. doi:10.1016/j.electacta.2017.05.185

Geioushy, R. A., Khaled, M. M., Hakeem, A. S., Alhooshani, K., and Basheer, C. (2017b). High efficiency graphene/Cu_2O electrode for the electrochemical reduction of carbon dioxide to ethanol. *J. Electroanal. Chem.* 785, 138–143. doi:10.1016/j.jelechem.2016.12.029

Gu, Z., Shen, H., Shang, L., Lv, X., Qian, L., and Zheng, G. (2018). Nanostructured copper-based electrocatalysts for CO_2Reduction. *Small Methods* 2 (11). doi:10.1002/smtd.201800121

Handoko, A. D., Ong, C. W., Huang, Y., Lee, Z. G., Lin, L., Panetti, G. B., et al. (2016). Mechanistic insights into the selective electroreduction of carbon dioxide to ethylene on Cu_2O-derived copper catalysts. *J. Phys. Chem. C* 120 (36), 20058–20067. doi:10.1021/acs.jpcc.6b07128

Hardebeck, J. L. (2015). Stress orientations in subduction zones and the strength of subduction megathrust faults. *Science* 349 (6253), 1213–1216. doi:10.1126/science.aac5625

Hori, Y., Takahashi, I., Koga, O., and Hoshi, N. (2002). Selective formation of C_2 compounds from electrochemical reduction of CO_2 at a series of copper single crystal electrodes. *J. Phys. Chem. B* 106 (1), 15–17. doi:10.1021/jp013478d

Hori, Y., Takahashi, I., Koga, O., and Hoshi, N. (2003). Electrochemical reduction of carbon dioxide at various series of copper single crystal electrodes. *J. Mol. Catal. A Chem.* 199 (1-2), 39–47. doi:10.1016/s1381-1169(03)00016-5

Jiang, K., Sandberg, R. B., Akey, A. J., Liu, X., Bell, D. C., Norskov, J. K., et al. (2018). Metal ion cycling of Cu foil for selective C-C coupling in electrochemical CO_2 reduction. *Nat. Catal.* 1 (2), 111–119. doi:10.1038/s41929-017-0009-x

Jung, H., Lee, S. Y., Lee, C. W., Cho, M. K., Won, D. H., Kim, C., et al. (2019). Electrochemical fragmentation of Cu2O nanoparticles enhancing selective C-C coupling from CO2 reduction reaction. *J. Am. Chem. Soc.* 141 (11), 4624–4633. doi:10.1021/jacs.8b11237

Kas, R., Kortlever, R., Milbrat, A., Koper, M. T., Mul, G., and Baltrusaitis, J. (2014). Electrochemical CO_2 reduction on Cu_2O-derived copper nanoparticles: controlling the catalytic selectivity of hydrocarbons. *Phys. Chem. Chem. Phys.* 16 (24), 12194–12201. doi:10.1039/c4cp01520g

Kim, D., Lee, S., Ocon, J. D., Jeong, B., Lee, J. K., and Lee, J. (2015). Insights into an autonomously formed oxygen-evacuated Cu_2O electrode for the selective production of C_2H_4 from CO_2. *Phys. Chem. Chem. Phys.* 17 (2), 824–830. doi:10.1039/c4cp03172e

Lee, S., Kim, D., and Lee, J. (2015). Electrocatalytic production of C_3 C_4 compounds by conversion of CO_2 on a chloride induced bi phasic Cu_2O Cu catalyst. *Angew. Chem.* 127 (49), 14914–14918. doi:10.1002/ange.201505730

Li, B., Nie, K., Zhang, Y., Yi, L., Yuan, Y., Chong, S., et al. (2023). Engineering single-layer hollow structure of transition metal dichalcogenides with high 1T-phase purity for hydrogen evolution reaction. *Adv. Mater* 35 (46), e2303285. doi:10.1002/adma.202303285

Li, C. W., and Kanan, M. W. (2012). CO_2 reduction at low overpotential on Cu electrodes resulting from the reduction of thick Cu2O films. *J. Am. Chem. Soc.* 134 (17), 7231–7234. doi:10.1021/ja3010978

Li, D., Huang, L., Tian, Y., Liu, T., Zhen, L., and Feng, Y. (2021). Facile synthesis of porous Cu-Sn alloy electrode with prior selectivity of formate in a wide potential range for CO_2 electrochemical reduction. *Appl. Catal. B Environ.* 292, 120119. doi:10.1016/j.apcatb.2021.120119

Li, D., Liu, T., Yan, Z., Zhen, L., Liu, J., Wu, J., et al. (2020). MOF-derived Cu_2O/Cu nanospheres anchored in nitrogen-doped hollow porous carbon framework for increasing the selectivity and activity of electrochemical CO_2-to-Formate conversion. *ACS Appl. Mater Interfaces* 12 (6), 7030–7037. doi:10.1021/acsami.9b15685

Liu, B., Yao, X., Zhang, Z., Li, C., Zhang, J., Wang, P., et al. (2021). Synthesis of Cu_2O nanostructures with tunable crystal facets for electrochemical CO_2 reduction to alcohols. *ACS Appl. Mater Interfaces* 13 (33), 39165–39177. doi:10.1021/acsami.1c03850

Liu, M., Pang, Y., Zhang, B., De Luna, P., Voznyy, O., Xu, J., et al. (2016). Enhanced electrocatalytic CO_2 reduction via field-induced reagent concentration. *Nature* 537 (7620), 382–386. doi:10.1038/nature19060

Liu, X., Xiao, J., Peng, H., Hong, X., Chan, K., and Norskov, J. K. (2017). Understanding trends in electrochemical carbon dioxide reduction rates. *Nat. Commun.* 8 (1), 15438. doi:10.1038/ncomms15438

Liu, Z., Nie, K., Qu, X., Li, X., Li, B., Yuan, Y., et al. (2022). General bottom-up colloidal synthesis of nano-monolayer transition-metal dichalcogenides with high 1t'-phase purity. *J. Am. Chem. Soc.* 144 (11), 4863–4873. doi:10.1021/jacs.1c12379

Loiudice, A., Lobaccaro, P., Kamali, E. A., Thao, T., Huang, B. H., Ager, J. W., et al. (2016). Tailoring copper nanocrystals towards C_2 products in electrochemical CO_2 reduction. *Angew. Chem. Int. Ed. Engl.* 55 (19), 5789–5792. doi:10.1002/anie.201601582

Lu, Q., Rosen, J., Zhou, Y., Hutchings, G. S., Kimmel, Y. C., Chen, J. G., et al. (2014). A selective and efficient electrocatalyst for carbon dioxide reduction. *Nat. Commun.* 5, 3242. doi:10.1038/ncomms4242

Obama, B. (2017). The irreversible momentum of clean energy. *Science* 355 (6321), 126–129. doi:10.1126/science.aam6284

Qin, X. P., Balbuena, P. B., and Shao, M. H. (2019). First-principles study on the initial oxidative decompositions of ethylene carbonate on layered cathode surfaces of lithium-ion batteries. *J. Phys. Chem. C* 123 (23), 14449–14458. doi:10.1021/acs.jpcc.9b02096

Ren, D., Deng, Y. L., Handoko, A. D., Chen, C. S., Malkhandi, S., and Yeo, B. S. (2015). Selective electrochemical reduction of carbon dioxide to ethylene and ethanol on copper(I) oxide catalysts. *Acs Catal.* 5 (5), 2814–2821. doi:10.1021/cs502128q

Ren, S. X., Joulie, D., Salvatore, D., Torbensen, K., Wang, M., Robert, M., et al. (2019). Molecular electrocatalysts can mediate fast, selective CO_2 reduction in a flow cell. *Science* 365 (6451), 367–369. doi:10.1126/science.aax4608

Ren, X., Zhang, X., Cao, X., and Wang, Q. (2020). Efficient electrochemical reduction of carbon dioxide into ethylene boosted by copper vacancies on stepped cuprous oxide. *J. CO_2 Util.* 38, 125–131. doi:10.1016/j.jcou.2020.01.018

Robb, A. M. (2021). Concentrated ethanol electrosynthesis from CO_2.

Roy, A., Jadhav, H. S., and Gil Seo, J. (2020). Cu_2O/CuO electrocatalyst for electrochemical reduction of carbon dioxide to methanol. *Electroanalysis* 33 (3), 705–712. doi:10.1002/elan.202060265

Shang, L., Lv, X., Shen, H., Shao, Z., and Zheng, G. (2019). Selective carbon dioxide electroreduction to ethylene and ethanol by core-shell copper/cuprous oxide. *J. Colloid Interface Sci.* 552, 426–431. doi:10.1016/j.jcis.2019.05.073

Su, W., Ma, L., Cheng, Q., Wen, K., Wang, P., Hu, W., et al. (2021). Highly dispersive trace silver decorated Cu/Cu_2O composites boosting electrochemical CO_2 reduction to ethanol. *J. CO_2 Util.* 52, 101698. doi:10.1016/j.jcou.2021.101698

Tan, W., Cao, B., Xiao, W., Zhang, M., Wang, S., Xie, S., et al. (2019). Electrochemical reduction of $CO_{(2)}$ on hollow cubic Cu(2)O@Au nanocomposites. *Nanoscale Res. Lett.* 14 (1), 63. doi:10.1186/s11671-019-2892-3

Tian, N., Zhou, Z. Y., Sun, S. G., Ding, Y., and Wang, Z. L. (2007). Synthesis of tetrahexahedral platinum nanocrystals with high-index facets and high electro-oxidation activity. *Science* 316 (5825), 732–735. doi:10.1126/science.1140484

Verdaguer-Casadevall, A., Li, C. W., Johansson, T. P., Scott, S. B., McKeown, J. T., Kumar, M., et al. (2015). Probing the active surface sites for CO reduction on oxide-derived copper electrocatalysts. *J. Am. Chem. Soc.* 137 (31), 9808–9811. doi:10.1021/jacs.5b06227

Wang, M., Ren, X., Yuan, G., Niu, X., Xu, Q., Gao, W., et al. (2020). Selective electroreduction of CO_2 to CO over co-electrodeposited dendritic core-shell indium-doped Cu@Cu_2O catalyst. *J. CO_2 Util.* 37, 204–212. doi:10.1016/j.jcou.2019.12.013

Wang, W., Ning, H., Yang, Z., Feng, Z., Wang, J., Wang, X., et al. (2019). Interface-induced controllable synthesis of Cu_2O nanocubes for electroreduction CO_2 to C_2H_4. *Electrochimica Acta* 306, 360–365. doi:10.1016/j.electacta.2019.03.146

Wang, Z., Yang, G., Zhang, Z., Jin, M., and Yin, Y. (2016). Selectivity on etching: creation of high-energy facets on copper nanocrystals for CO_2 electrochemical reduction. *ACS Nano* 10 (4), 4559–4564. doi:10.1021/acsnano.6b00602

Wu, D., Wang, X., Fu, X.-Z., and Luo, J.-L. (2020). Ultrasmall Bi nanoparticles confined in carbon nanosheets as highly active and durable catalysts for CO_2 electroreduction. *Appl. Catal. B Environ.* 284, 119723. doi:10.1016/j.apcatb.2020.119723

Zhang, W., Qin, Q., Dai, L., Qin, R., Zhao, X., Chen, X., et al. (2018). Electrochemical reduction of carbon dioxide to methanol on hierarchical Pd/SnO2 nanosheets with abundant Pd–O–Sn interfaces. *Angew. Chem. Int. Ed.* 57 (30), 9475–9479. doi:10.1002/anie.201804142

Zhang, Y., Li, K., Chen, M., Wang, J., Liu, J., and Zhang, Y. (2019). Cu/Cu_2O nanoparticles supported on vertically ZIF-L-coated nitrogen-doped graphene nanosheets for electroreduction of CO_2 to ethanol. *ACS Appl. Nano Mater.* 3 (1), 257–263. doi:10.1021/acsanm.9b01935

Zhao, Z., Wang, X., Si, J., Yue, C., Xia, C., and Li, F. (2018). Truncated concave octahedral Cu_2O nanocrystals with {hkk} high-index facets for enhanced activity and stability in heterogeneous catalytic azide–alkyne cycloaddition. *Green Chem.* 20 (4), 832–837. doi:10.1039/c7gc03020g

Zhi, W.-Y., Liu, Y.-T., Shan, S.-L., Jiang, C.-J., Wang, H., and Lu, J.-X. (2021). Efficient electroreduction of CO_2 to C_2-C_3 products on Cu/Cu_2O@N-doped graphene. *J. CO_2 Util.* 50, 101594. doi:10.1016/j.jcou.2021.101594

Zhu, S., Ren, X., Li, X., Niu, X., Wang, M., Xu, S., et al. (2021). Core-Shell ZnO@Cu_2O as catalyst to enhance the electrochemical reduction of carbon dioxide to C_2 products. *Catalysts* 11 (5), 535. doi:10.3390/catal11050535